I&EC research
Industrial & Engineering Chemistry Research

Article

pubs.acs.org/IECR

Artificial Neural Networks, Optimization and Kinetic Modeling of Amoxicillin Degradation in Photo-Fenton Process Using Aluminum Pillared Montmorillonite-Supported Ferrioxalate Catalyst

O. B. Ayodele,*[,†,§] H. S. Auta,[‡] and N. Md Nor[†]

[†]School of Chemical Engineering, Engineering Campus, University of Science Malaysia, 14300 Nibong Tebal, Penang, Malaysia
[‡]Department of Microbiology, Federal University of Technology, Minna, Nigeria
[§]Department of Chemical Engineering, University of Malaya, 50603 Kuala Lumpur, Malaysia

Supporting Information

ABSTRACT: An artificial neural network (ANN) was applied to study the hierarchy of significance of process variables affecting the degradation of amoxicillin (AMX) in a heterogeneous photo-Fenton process. Catalyst and H_2O_2 dosages were found to be the most significant variables followed by degradation time and concentration of AMX. The significant variables were optimized and the optimum condition to achieve degradation of 97.87% of 40 ppm AMX was 21.54% excess H_2O_2 dosage, 2.24 g of catalyst in 10 min. A mathematical model (MM) for the degradation of AMX was developed on the basis of the combined results of the ANN and the optimization studies. The MM result showed that increases in both catalyst and H_2O_2 dosage enhanced the rate of AMX degradation as shown by the rate constants evaluated from the model. The highest rate constant at the optimum conditions was 122 M^{-1} S^{-1}. These results provided invaluable insights into the catalytic degradation of AMX in photo-Fenton process.

1. INTRODUCTION

Amoxicillin (AMX) is an antibiotic that belongs to the penicillin class and is used in both veterinary and human medicine.[1] It belongs to the class of the most prescribed antibiotics in both developing and developed because of its high-therapeutic efficiency at blocking the biosynthetic enzymes that compose the cell walls of bacteria due to the presence of broad-spectrum β-lactam rings.[1,2] The major problem that is created by the presence of AMX at low concentration in the environment is the development of antibiotic resistant bacteria.[3] AMX is a highly recalcitrant pollutant that cannot be easily degraded by conventional wastewater treatment methods like adsorption or biological and even the chemical oxidation methods,[4−6] but with the advent of Fenton, Fenton-like and photo-Fenton processes, AMX and other refractory pollutants have been conveniently degraded and mineralized completely under mild reaction condition.[5,6] The efficiency of a typical photo-Fenton process is strongly influenced by the iron (catalyst) loading, oxidant dosage, pollutant initial concentration, treatment time, and temperature. Therefore, for the purpose of gaining more insights into the photo-Fenton process application in wastewater treatment, the use of an artificial neural network to determine or ascertain process variables that strongly affect the pollutants degradation process cannot be over emphasized.[7−10] In addition, each of the parameters should be optimized for efficient treatment of wastewater[8−12] especially when mathematical model of the degradation kinetics is of interest.

Owing to the complexity of the photo-Fenton process, it is relatively difficult to model and simulate the degradation process using conventional mathematical methods, hence an artificial neural network (ANN) has now been introduced because of its simplicity toward modeling, simulation, and prediction,[3] and it is considered a promising tool. Its ability to recognize and reproduce cause−effect relationships through training for multiple input−output systems makes it efficient in representing even the most complex systems,[9] and it is more advantageous since the mathematical description of the phenomena involved in the process is not required. It also required lesser time with limited numbers of experiments for model development compared to the traditional mathematical models.[13,14] Application of ANN to solve environmental engineering problems ranging from biological wastewater treatment to advanced oxidation processes (AOPs) has been recently reported in literature.[9,13−16]

Similarly, due to the complex systems of the photo-Fenton catalytic degradation process, application of a one-factor-at-a-time-optimization approach could mislead the optimization process because of the lack of cross-factor effects.[9] Thus, the application of the design of experiments (DOE) seems to be an alternative option. There are different types of DOE available that usually require a number experiment and they are highly cost-effective and statistically reliable.[11] A good example of such methods that consider the simultaneous varying of influencing process parameters and still take into account the interactions between them is referred to as a response surface methodology (RSM).[12] However, the use of combined ANNs and RSM to study and optimize the factors that strongly affect the degradation process of a pollutant for the purpose of developing a phenomenological mathematical model of a pollutants degradation process is scarce in the literature.

Received: September 5, 2012
Revised: November 5, 2012
Accepted: November 23, 2012
Published: November 23, 2012

dx.doi.org/10.1021/ie302390b | *Ind. Eng. Chem. Res.* 2012, 51, 16311−16319

In this study, ANN and RSM modeling techniques were used to establish the relationship between AMX degradation process variables (catalyst dosage, hydrogen peroxide dosage, time, and initial AMX concentration) and output variable (degradation efficiency). The choice of the parameters was based on the previous report.[17] In the first step, the process variables were fed as inputs to an ANN with AMX degradation efficiency as the output of the network. The significance of each input variable on the output response was determined. Second, D-Optimal design a form of RSM was used to optimize the significant process variables, and finally, a phenomenological mathematical model for AMX degradation process was developed on the basis of the ANN and the RSM results.

2. EXPERIMENTAL SECTION

2.1. Materials and Methods. Montmorillonite clay (Neimenggu, China) with a cation exchange capacity (CEC) of 108.4 mequiv/100 g of clay was purchased from Sigma Aldrich Co. Analytical grade Amoxicillin trihydrate and hydrogen peroxide (H_2O_2) solution (30%) were obtained from Fluka. The iron hydroxide, oxalic acid, aluminum trichloride, and phosphoric acid were purchased from Merck (Germany), and polyvinyl alcohol was obtained from Sigma. The aluminum pillared montmorillonite catalyst (AlPMC) was prepared by direct dissolution of aluminum pillared montmorillonite (AlPM) precursor used as support with ferrioxalate (FeOx) complex prepared from iron hydroxide and oxalic acid. The details of the catalyst preparation were earlier reported.[17]

2.2. Experimental Procedure. A 1.0-L beaker filled with 500 mL of AMX was used as the Fenton reactor, and it was placed in a water-partly filled 2.0-L beaker situated on a hotplate with variable magnetic stirrer equipped with a temperature monitor and control facilities. Prior to the commencement of the Fenton process, the initial pH of the aqueous solution of AMX was measured and found to be 5.03, in the course of the reaction it decreased due to the formation of H_2SO_4 and HNO_3. After the addition of the AlPMC to the AMX solution, the UV lamp (Unilux Philips lamps 15W, λ_{max} = 254 nm) was switched on and the reaction was initiated by adding the required dosage of HP under a predetermined optimal magnetic stirring speed of 340 rpm. At selected time intervals, samples of the reaction mixture were taken with a syringe and filtered through a 0.45 μm membrane for analysis in a UV−vis spectrophotometer.

2.3. Analytical Methods. The maximum absorbance wavelength (λ_{max}) of AMX recorded from 500 to 200 nm using a spectrophotometric quartz cell in a UV−vis spectrophotometer (Shimadzu, model UV 1700 PharmaSpec, Japan) was found at 274 nm. The withdrawn filtered samples were quickly analyzed to minimize experimental errors since the reaction could still continue after withdrawal. The degradation efficiency (DE) of AMX was evaluated as follows:

$$\mathrm{DE}\% = \left[\frac{C_o - C_t}{C_o}\right]100 \tag{1}$$

where C_o and C_t are the initial concentration and the measured concentration of AMX at the time of withdrawal, respectively.

3. EXPERIMENTAL DESIGN

3.1. Artificial Neural Network. The artificial neural network for computational studies consists of simple processing units called neurons and each network consists of artificial neurons grouped into layers and put in relation to each other by parallel connections.[9] The strength of these interconnections is determined by the weight associated with the neurons.[3,9] The multilayer feed-forward net is a parallel interconnected structure consisting of an input layer which includes independent variables and an output layer; in between them is one or more neuron layers called hidden layers.[3] The number of variables used in the prediction and the number of variables to be predicted are represented by the number of input and output neurons, respectively. The degree of accuracy in the neural predictions is a function of the number of neurons in the hidden layer which acts like feature detectors, and there can be more than one hidden layer. On the basis of the theory of approximation, with a sufficiently large number of neurons, a network with a single hidden layer can interpret any input−output structure, and the most widely reported transfer function for the input and hidden layers is the sigmoid transfer function (eq 2) while the linear activation function (eq 3) is used as the output layer activation function.[9,14−16]

$$f(x) = \frac{1}{1 + e^x} \tag{2}$$

$$f(x) = \mathrm{x} \tag{3}$$

A mono hidden layer multilayer feed forward ANN is applied in this study. Sigmoidal activation function and a linear transfer function were used in the hidden layer and in the output node, respectively, for all the data sets. All calculations are carried out with Matlab mathematical software v 7.2 with ANN toolbox for training the ANNs using feed-forward neural network trained by the back-propagation (BP) algorithm. The independent variables earlier reported[17] were used as the input variables to the network. The variables were assigned the following notations: H_2O_2 dosage, $p1$; catalyst dosage, $p2$; time, $p3$ and initial AMX concentration, $p4$, while the AMX degradation efficiency was assigned the output variable.

3.2. Response Surface Methodology. A four factor D-Optimal design was used to determine the optimum operating conditions for maximizing the efficiency of the AMX degradation process. The four factors selected as independent variables based on previous experience and also as a prerequisite for process/product design of AMX treatment facility for industrial applications are H_2O_2 dosage, catalyst loading, time of degradation, and the initial concentration of AMX. They are assigned with DOE notation for independent variables as X_1, X_2, X_3 and X_4 respectively. Other parameters such as agitation speed and temperature were set at predetermined values based on previous experience. The pH was not adjusted because FeOx catalysts were able to achieve degradation at the natural pH (5.03) of AMX due to the presence of the ferrioxalate ligands.[17−19] Temperature of reaction was maintained at 30 ± 2 °C. The objective function to be optimized is degradation efficiency of AMX and is denoted as Y. Application of D-Optimal design as an optimization technique demands selections of a model at the beginning, in this particular case study, quadratic model was chosen as shown in eq 2. The adequacy of the final model was verified by graphical and numerical analysis.

$$\begin{aligned} Y = {} & b_0 + b_1X_1 + b_2X_2 + b_3X_3 + b_4X_4 + b_{12}X_1X_2 \\ & + b_{13}X_1X_3 + b_{14}X_1X_4 + b_{23}X_2X_3 + b_{24}X_2X_4 + b_{34}X_3X_4 \\ & + b_{124}X_1X_2X_4 + b_1{X_1}^2 + b_2{X_2}^2 + b_3{X_3}^3 \end{aligned} \tag{4}$$

dx.doi.org/10.1021/ie302390b | Ind. Eng. Chem. Res. 2012, 51, 16311−16319

where b_n is the coefficient associated with each nth factor, and combination of factors (such as X_1X_2) represents interactions between the individual factors in that term.

The number of experiments for four independent variables was calculated as follows according to DOE configuration using Design-Expert 7.1.6 from Stat Ease Inc.: minimum model points, 15; lack of fits estimate points, 5; replicates points, 5; additional center points, 0; total experiments, 25. The model obtained was evaluated for the response function and the experimental data were analyzed statistically applying analysis of variance (ANOVA).

4. RESULTS AND DISCUSSION

4.1. Degradation of AMX/UV/H_2O_2/AlPMC Process. A classical and systematic sequential approach was followed for the degradation of AMX to determine the range (−1 to +1) of values of the independent variables to be used in the design of experiment for the optimization studies. The degradation process was first carried out without catalyst in a stoichiometric ratio of eq 5 and followed by 10, 15, 20, and 25% excess H_2O_2, and the process efficiency was monitored and recorded. The best experimental condition was identified and repeated with different AlPMC dosage. Finally, the range of best H_2O_2 dosage and AlPMC loading was investigated with different initial concentration of AMX. The range of all experimental input variables are shown in Table S1 (online Supporting Information).

$$C_{16}H_{19}N_3O_5S + 47H_2O_2 + Fe^{2+} \rightarrow 16CO_2 + 54H_2O + 3HNO_3 + H_2SO_4 + Fe^{2+} \quad (5)$$

4.2. Artificial Neural Networks (ANN) Model Development. The H_2O_2 dosage, catalyst loading, treatment time and initial concentration of AMX were all found to affect the degradation of AMX in the previous report.[17] Hence, there is need for ANN studies to establish the hierarchy of significance of these input variables.

4.2.1. Selection of Back-Propagation (BP) Training Algorithm. Ten different BP algorithms were studied in order to determine the best BP training algorithm. Tangent sigmoid transfer function (tansig) and a linear transfer function (purelin) were used at the hidden and output layers, respectively. The result of comparisons among the different BP training algorithms (for those with R^2 greater than 0.9) is shown in Table S2 (see online Supporting Documents). Levenberg−Marquardt back-propagation algorithm (LMA) was chosen in this study as the training algorithm because among the algorithms with a very high degree of correlation (R^2), it has the least mean square error (MSE). The MSE measures the performance of the network using eq 6.

$$\mathrm{MSE} = \frac{\sum_{i=1}^{i=N} (y_{i,\mathrm{pred}} - y_{i,\mathrm{expt}})^2}{N} \quad (6)$$

where N is the number of data points, $y_{i,\mathrm{pred}}$ and $y_{i,\mathrm{expt}}$ is the network prediction and experimental response, respectively, while i is an index of data.

4.2.2. Optimization of the Neurons Number. A series of network architecture was used to determine the optimum number of hidden nodes, in which the number of nodes was varied from 2 to 20 as shown in Figure 1. The mean square error (MSE) was used as the error function and plotted against the number of neurons prediction set. ANN optimization

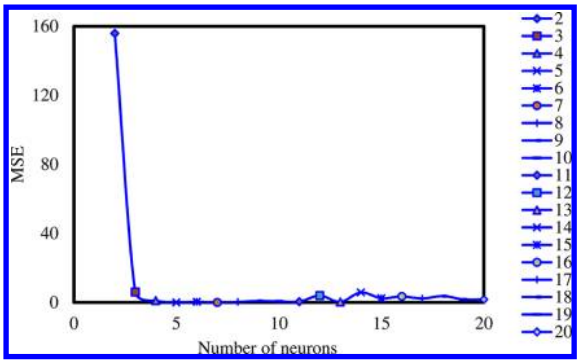

Figure 1. Effect of number of the hidden neurons on performance of the neural network.

process required network training to minimize the error function (MSE) by searching for a set of connection weights that can enable the ANN to produce outputs that are identical or possibly equal to target values.[3] It can be seen that with two neurons, the MSE was 155.94; the value decreased to 0.0015 when the number of neurons were increased to 5. Further increment in the number of neurons from 5 to 11 does not significantly decrease the MSE, and the MSE increased when the numbers of neurons were increased beyond 12. On the basis of this observation, the tangent sigmoid transfer function (tansig) at the hidden layer with five neurons and linear transfer function (purelin) at the output layers were used for the modeling of the AMX degradation process.

4.2.3. Testing and Validation of the Developed Model. The results of the validity of the ANN tested by comparing its predicted output values with the experimental values at 20, 40, and 60 ppm initial concentration of AMX using independent set of data is shown in Figure 2. The result showed two types of

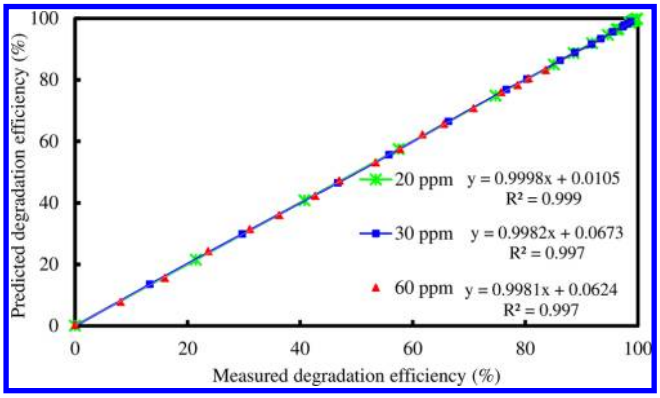

Figure 2. Comparison between predicted and experimental values of the output.

line with a high degree of correlation; the first is the perfect fit $y = x$ (predicted data = experimental data) and the others are 20, 40, and 60 ppm AMX. The three concentrations tested showed very high correlation (R^2) which increased from 0.997 to 0.999 as the initial concentration is decreased from 60 to 20 ppm. This result is in agreement with what has been reported earlier in the literature. Elmolla et al.[3] reported 0.997 in the degradation of amoxicillin, ampicillin, and cloxacillin in the homogeneous photo-Fenton process, and Kasiri et al.[9] reported 0.998 in the degradation of C.I. Acid Red 14 azo dye using Fe-ZSM5.

4.2.4. Determination of the Significance of Each Input Variable on the Output Variables. To evaluate the relative importance of the input variables, neural net weight matrix and Garson equation were used in the evaluation processes. Garson proposed the equation based on the partitioning of connection weights as shown in eq 7. The weights are coefficients between the artificial neurons, which are analogous to synapse strengths between the axons and dendrites in real biological neurons.[3,9] Consequently, each weight decides what ratio of the incoming signal will be transmitted into the neuron's body.[20] The neural net weight matrix can be used to assess the relative significance of the various input variables on the output variable:

$$Ij = \frac{\sum_{m=1}^{m=N_h}\left(\left(\frac{|W_{jm}^{ih}|}{\sum_{m=1}^{m=N_h}|W_{km}^{ih}|}\right)|W_{mn}^{ho}|\right)}{\sum_{m=1}^{m=N_h}\left\{\sum_{m=1}^{m=N_h}\left(\frac{|W_{jm}^{ih}|}{\sum_{k=1}^{N_i}|W_{km}^{ih}|}\right)|W_{mn}^{ho}|\right\}} \quad (7)$$

where, Ij is the relative significance of the jth input variable on the output variable, N_i and N_h are the number of input and hidden neurons, respectively. W is connection weight, the superscripts "i" "h" and "o" represents the input, hidden, and output layers, respectively, while the subscripts "k", "m" and "n" refer to input, hidden, and output neurons, respectively.[3]

The relative significance of the four input variable computed by the Garson equation showed that H_2O_2 dosage and AlPMC loading are the most significant variables with 30.07 and 31.02%, repectively, followed by the treatment time (25.09%), and finally the initial concentration of the AMX (13.79). The higher significance of H_2O_2 dosage and AlPMC loading observed was in consonance with the trend in the photo-Fenton process of wastewater treatment.[3,9,20] This strong significance may be because the two variables have both linear and polynomial effects on the degradation process (as revealed by response surface plots); that is, the initial increase in their values enhanced the degradation efficiency up to the optimum point where further increment decreased the degradation efficiency due to scavenging effect of the excess H_2O_2 and AlPMC loading on the reactive $HO^{\bullet}$[4] according to eq 8−10. The lower relative importance of antibiotic concentration showed that the selected H_2O_2 dosage and AlPMC loading are valid for the range of AMX simulated wastewater studied.[3]

$$H_2O_2 + HO^{\bullet} \rightarrow HO_2^{\bullet} + H_2O \quad (8)$$

$$HO^{\bullet} + HO^{\bullet} \rightarrow H_2O_2 \quad (9)$$

$$Fe^{2+} + HO^{\bullet} \rightarrow Fe^{3+} + OH^{-} \quad (10)$$

The second evaluation process is based on the possible combination of variables that were examined by the optimal ANN structure using the LMA with 5 hidden neurons. The result for the sensitivity analysis for different possible combinations is available in the Supporting Information (Table S3). The result showed that p2 (AlPMC loading) was the most effective parameter among other input variables in the group of one variable, this is also in agreement with the result of the Garson equation. The MSE (323.93) decreased to 314.52, 157.21, and 43.73 when combined with p1, p3, and p4, respectively. This emphasized its significance on the degradation process. Similarly, in the group of single variables, p1 has an MSE of 457.49 which is next to p2. The value decreased drastically to 314.52, 69.65, and 138.22 when combined with p2, p3, and p4, respectively. The significance of p2 is observed to be prevalent in all the combinations as already noted, its MSE decreased to 43.73 which is the minimum in the group of two. Its MSE further decreased to 3.83 when combined with p3 and p4, which also is the minimum in the group of three. It can be concluded therefore that the contribution of p1 and p2 were responsible for the drastic reduction in the MSE to 0.46 when all input variables are combined together. In addition, it can be seen that all variables were significant on their own merit and this is in accordance with the sensitivity test using the Garson equation.

4.3. D-Optimal Experimental Design. *4.3.1. Development of Regression Model Equations.* Having established the significance of the input variables, there is additional need to optimize the AMX degradation process especially for the most significant variables (H_2O_2 dosage and AlPMC loading). To achieve this, a total of 25 experiments were performed for the construction of the experimental design according to D-Optimal design and their results are shown in Supporting Information, Table S4. The coefficients of independent variables (X_1, X_2, X_3, and X_4) and their interaction effects on the response functions, Y (AMX degradation) were determined. The corresponding statistical polynomials model was obtained by multiple regressions and is shown in eq 11.

$$\begin{aligned}\%\text{AMX degradation } (Y) &= -110.39 + 20.92X_1 + 54.13X_2 + 6.96X_3 - 1.12X_4 \\ &\quad - 0.92X_1^{\,2} - 13.50X_2^{\,2} - 0.29X_3^{\,2} + 1.8 \times 10^{-4}X_4^{\,2} \\ &\quad - 0.29X_1X_2 + 0.05X_1X_3 + 0.03X_1X_4 + 0.11X_2X_3 \\ &\quad + 5.3 \times 10^{-4}X_2X_4 + 0.03X_3X_4 \end{aligned} \quad (11)$$

4.3.2. Analysis of Regression Model Equations. A comparison between the model prediction and the experimental response parity plots (see Figure S1 in the Supporting Information) showed a reasonable degree of agreement validating the second-order polynomial model applied. The experimental error observed between the predicted and experimental response functions is very negligible which showed that there is a strong correlation between the independent variable and the response function. To corroborate this, the analysis of variance (ANOVA) was used test the goodness of fit for the polynomial coefficients of the response function (AMX degradation), and the results are presented in Table S5 (Supporting Information). The mean squares were obtained by dividing the sum of squares for each variation by their respective degrees of freedom while the F-value was calculated by dividing the obtained mean squares with the residual mean square (7.34). The model F-value is 110.04 for the AMX response function (Y). This implied that the models are significant, and there is only a 0.01% chance that model F-values this large could occur due to model error,[21] although it may be associated to experimental error. Values of "Prob > F" less than 0.0500 indicated that model terms are significant. In this case X_1, X_2, $X_1^{\,2}$, $X_2^{\,2}$, and $X_3^{\,2}$ are significant model terms, which is a confirmation of the result of the ANN that showed p1 and p2 to be the most significant input variable. The obtained regression coefficient (R^2) is 0.9932 and the adjusted regression coefficient ($R_{adj}^{\,2}$), that corrects R^2 for the sample size and the number of terms in the models is 0.9838. Generally, if a mode contains many terms and has a small sample size this could result in a much lower $R_{adj}^{\,2}$ compared to R^2;[7,22] in this case the model has high R^2 and $R_{adj}^{\,2}$ which

confirmed that the chosen quadratic models in the D-Optimal design for the response surface method adequately described the Experimental data in the range of the operating parameters.

Finally, two important pieces of information to investigate any deficiency or descrepancy in the model fitting to the experimental data on the performance of the model can be seen in the plot of internally studentized residuals vs normal probability (see Figure S2a in the Supporting Information) and the plot of run number vs outlier T points (see Figure S2b in the Supporting Information). The normal probability plot showed orchestrated points and points cluster in close neighborhood of the diagonal line, an indication of the homogeneousity of the error variances and independent style of the residuals which confrimed that errors are normally distributed and independent of each other.[11,21−23] From the plot of run numbers vs outlier's T points, which can be used to evaluate the assumption of constant variance, it was observed that the points are randomly scattered and structureless which confirm that all the information is well extracted and the residuals are unrelated to any other variables.[4,23] All the outlier's T points lay well within the range of −3.5 to +3.5, which is considered as the bottom and top outlier detection limits. Since all the points were captured within this range, it can be concluded that the response transformation is appropriate and successful in capturing the correlation between the four studied parameters influencing the degradation of AMX without any apparent problem with the normality. From the various analysis studied, it can be seen that the quadratic model adequately and successfully captured and described the AMX degradation processes; hence it was applied for the RSM and optimization study.

4.3.3. Response Surface Plots. 4.3.3.1. Effect of AlPMC Loading and H_2O_2 Dosage. The response plot for the effect of AlPMC loading and H_2O_2 dosage (Figure 3) showed that the degradation of AMX is enhanced by an increase in H_2O_2 concentration from 15 up to 20% excess H_2O_2, but a decrease in degradation rate was observed when the amount of H_2O_2 was further increased to 25% excess H_2O_2. This is probably due to the scavenging effect of H_2O_2 on the reactive $HO^•$ as shown in eq 8 to form the hydroperoxy radical ($HO_2^•$) with a lower reactivity and oxidation potential of 1.7 eV compared to 2.8 eV of the $HO^•$. Excess H_2O_2 could also generate excess $HO^•$ radicals that undergo dimerism to form H_2O_2 according to eq 9. These cumulative effects were believed to be responsible for the reduction in the response function Y (degradation rate of AMX).

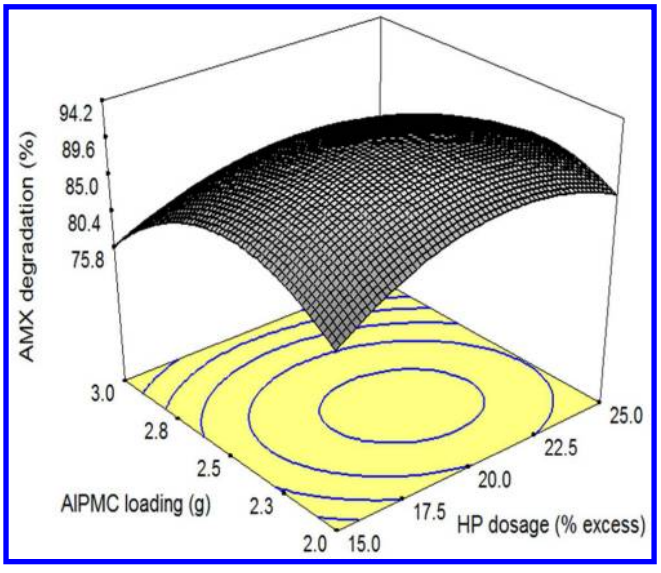

Figure 3. Response surface plots for degradation of AMX using AlPMC; $[AMX]_o$ = 40 ppm, temperature = 30 °C, time = 8 min.

Similarly, the effect of AlPMC loading on the response function Y showed a significant increase in the degradation of AMX as the catalyst dosage is increased from 2.0 to 2.5 g. This is due to the increase in the rate of $HO^•$ generation as more active sites were available for the catalytic hydroxylation of H_2O_2 at a faster rate. On the contrary, when catalyst loading was increased to 3.0 g, degradation efficiency decreases due to the inhibition effect of excess iron ions that act as scavengers on the $HO^•$ in the photo-Fenton process as shown in eq 10. It can be seen that the plots are predominantly quadratic as revealed by the contour lines on the H_2O_2 dosage−AlPMC loading plane. This further confirmed that the quadratic model earlier chosen adequately described the degradation process. These observations are at par with the established trend in the literature.[22−27]

4.3.3.2. Effect of Initial Concentration of AMX and Time. The response plot for the effect of initial concentration of AMX and time in Figure 4 shows that both factors affect the degradation efficiency. At a higher initial concentration of AMX, the degradation efficiency is low but it increased as the initial concentration of AMX is reduced. This is because as the initial concentration was increased other factors affecting the rate of degradation were not simultaneously increased, thereby making the available $HO^•$ insufficient for the degradation of the AMX pollutant. The degradation efficiencies increased as the reaction time increased at both low and high initial concentrations of AMX. At about 8 min of reaction time, 20 ppm initial concentration of AMX showed a parallel plot with the time axis. This implied that any treatment beyond that time may not reflect in further degradation based on the experimental conditions. The parallel plot diminished toward the positive side of the AMX concentration axis and showed an inflection around 40 ppm initial concentration. This suggested that the process parameter conditions for any concentration of AMX below this point of inflection could be in excess of the requirement, but definitely not sufficient for concentration

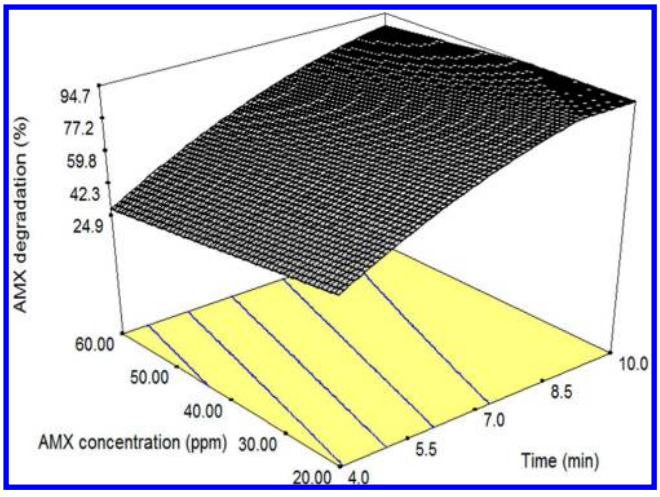

Figure 4. Response surface plots for degradation of AMX; AlPMC loading = 2.5 g, H_2O_2 dosage = 20% excess, temperature = 30 °C.

above it, as the degradation efficiency is seen to reduce as the initial concentration of AMX approached 60 ppm. Hence there is a need to optimize to get the exact process requirement for a given concentration.

4.3.4. Optimization (Desirability Plot) and Validation of Results. The optimized degradation conditions of AMX based on the interaction between the independent factors were plotted as contour lines and the desirability increased toward the center of the plot as shown in Figure 5. The best desirability

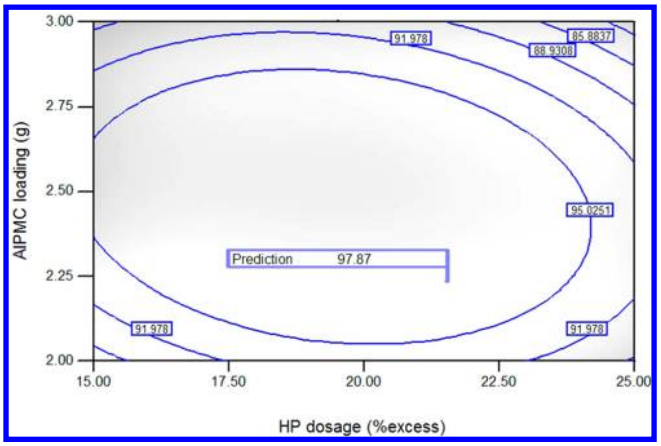

Figure 5. Desirability plot for the degradation of AMX using AlPMC.

point on the contours gave the optimum condition to achieve 97.87% degradation of 40 ppm of AMX to be 21.54% excess H_2O_2, 2.24 g of AlPMC in 10 min reaction time. The optimization result was validated in a repeated experiment and the average degradation efficiency is shown in Table 1. The result showed 2.47% variation between the predicted and the observed experimental degradation efficiencies of AMX. However, since the adequacy of the quadratic model had earlier been validated, this variation could be ascribed to human error during experimental studies. Consequently, these optimization results in conjunction with the results of ANN were used for the development of mathematical model for the kinetics of AMX degradation studies.

4.4. Kinetic Modeling for Degradation of AMX in Photo-Fenton Process. *4.4.1. Model Development.* A typical photo-Fenton process has three major reaction stages: chain initiation, chain propagation and chain termination. Although there are many possible reaction that may take place during photo-Fenton process, the following are the most predominantly accepted and used in literature since 1930s when the mechanisms of $HO^\bullet$ were first proposed and studied because they adequately describe all the three stages.[10]

Stage 1, chain initiation:

$$Fe^{2+} + H_2O_2 \rightarrow Fe^{3+} + HO^\bullet + OH^- \quad (k_1 \approx 70.0\ M^{-1}\ s^1) \tag{R1}$$

Stage 2, chain propagation:

$$AMX + HO^\bullet \rightarrow CO_2 + H_2O + \text{mineral products (dependent on the pollutant)} \tag{R2}$$

$$HO^\bullet + H_2O_2 \rightarrow H_2O + HO_2^\bullet \quad (k_3 = 3.3 \times 10^7\ M^{-1}\ s^{-1}) \tag{R3}$$

$$H_2O_2 + Fe^{3+} \rightarrow Fe^{2+} + {}^\bullet HO_2 + H^+ \quad (k_4 = 0.01\ M^{-1}\ s^{-1}) \tag{R4}$$

$$Fe^{3+}(OH^-) + h\nu \rightarrow Fe^{2+} + HO^\bullet \quad (k_{(UV)} = \text{variable depending on } h\nu \text{ intensity}) \tag{R5}$$

$$Fe^{3+} + HO_2^\bullet \rightarrow Fe^{2+} + O_2 + H^+ \quad (k_6 = 1.2 \times 10^6\ M^{-1}\ s^{-1}) \tag{R6}$$

Stage 3, chain termination:

$$Fe^{2+} + HO^\bullet \rightarrow Fe^{3+} + HO^- \quad (k_7 = 3.2 \times 10^8\ M^{-1}\ s^{-1}) \tag{R7}$$

$$Fe^{2+} + HO_2^\bullet \rightarrow Fe^{3+} + HO_2^- \quad (k_8 = 1.3 \times 10^6\ M^{-1}\ s^{-1}) \tag{R8}$$

In the degradation of AMX in photo-Fenton process, the degradation is caused by the $HO^\bullet$ attack on the AMX molecule and subsequent opening of its β-lactam ring.[6,17] Therefore, it can be concluded that AMX is primarily degraded in these studies due to $HO^\bullet$ generation at the AlPMC active sites as earlier noted elsewhere. At the completion of the photo-Fenton process, the amount of the H_2O_2 is considered zero, since Fenton catalysts have not been reported to suffer from any severe deactivation or poisoning that can halt the generation of the $HO^\bullet$.

The rate equation for AMX degradation can be represented as

$$\Gamma_{AMX} = -\frac{d[AMX]}{dt} = k_2[AMX][HO^\bullet] \tag{12}$$

Similarly, the rate of $HO^\bullet$ consumption can be represented as

$$\frac{d[HO^\bullet]}{dt} = k_1[Fe^{2+}][H_2O_2] - k_2[HO^\bullet][AMX] - k_3[HO^\bullet][H_2O_2] - k_7[HO^\bullet][Fe^{2+}] \tag{13}$$

From the optimization process, overdosing the reaction with H_2O_2 had been prevented; hence the effect of R3 can be eliminated. As discussed earlier, an increase in the H_2O_2 dosage from 10 to 20% excess H_2O_2 enhanced the degradation of AMX. A decrease in degradation rate was observed when the H_2O_2 dosage was increased to 25% excess due to the scavenging effect of H_2O_2 on the $HO^\bullet$ to form hydroperoxy

Table 1. Validation of the Optimization Result for AMX Degradation with AlPMC

factors				AMX degradation (%)		
H_2O_2 dosage (% excess)	AlPMC loading (g)	time (min)	AMX concentration (ppm)	predicted (%)	experimental (%)	residual (%)
21.54	2.24	10.0	40	97.87	95.4	2.47

dx.doi.org/10.1021/ie302390b | *Ind. Eng. Chem. Res.* 2012, 51, 16311−16319

radical ($HO_2^{\bullet}$) whose reactivity and oxidation potential is lower compared to $HO^{\bullet}$. The optimization process achieved an optimum value of 21.54% between 20 and 25% excess H_2O_2 with a comparably higher AMX degradation efficiency of 97.87%. Therefore, eq 13 can be reduced to

$$\frac{d[HO^{\bullet}]}{dt} = k_1[Fe^{2+}][H_2O_2] - k_2[HO^{\bullet}][AMX] - k_7[HO^{\bullet}][Fe^{2+}] \quad (14)$$

The rate of H_2O_2 and Fe^{2+} disappearance can be written as

$$\frac{d[H_2O_2]}{dt} = -k_1[Fe^{2+}][H_2O_2] - k_3[HO^{\bullet}][H_2O_2] - k_4[Fe^{3+}][H_2O_2] \quad (15)$$

$$\frac{d[Fe^{2+}]}{dt} = -k_1[Fe^{2+}][H_2O_2] - k_4[Fe^{3+}][H_2O_2] - k_6[Fe^{3+}][HO_2^{\bullet}] - k_7[Fe^{2+}][HO^{\bullet}] - k_8[Fe^{2+}][HO_2^{\bullet}] \quad (16)$$

It is worth noting that the application of UV irradiation to photoreduce Fe^{3+} to Fe^{2+} will have an overriding effect on R4 as earlier reported[17] such that R4 is employed to reduce Fe^{3+} to Fe^{2+} in the absence of UV irradiation. Consequently, R4 can also be eliminated more so because its rate constant is extremely small compared to other constants. Similarly, since $k_8 \ll k_7$ in the termination stage, that is, a comparably lower rate constant, R8 can be ignored,[10,28,29] and more importantly the generation of $HO_2^{\bullet}$ required for the reaction in R8 was inhibited by the optimization process R3 and photoirradiation R4. This also affected R6, hence it can also be ignored coupled with the fact that the application of UV irradiation is assumed to have photoreduced all Fe^{3+} to Fe^{2+} in either classical photo-Fenton process R5 or ferrioxalate photochemistry (eq 17) as soon as they are generated.

$$Fe^{III}(C_2O_4)_n^{(3-2n)+} + h\nu \rightarrow Fe^{2+} + (n-1)C_2O_4^{2-} + C_2O_4^{\cdot -} \qquad n = 1, 2, \text{ or } 3 \quad (17)$$

Considering the above process constraints and noting that $k_1 \ll k_7$ in eq 16, eq 15 and eq 16 can be rewritten as

$$\frac{d[H_2O_2]}{dt} = -k_1[Fe^{2+}][H_2O_2] \quad (18)$$

$$\frac{d[Fe^{2+}]}{dt} = -k_7[Fe^{2+}][HO^{\bullet}] \quad (19)$$

Since the $HO^{\bullet}$ is a very reactive radical and possess a limited lifespan of nanoseconds, it can only be used up immediately upon generation, therefore its concentration can be considered constant throughout the propagation stage and its rate of change approaches zero;[10,29] i.e., $d[HO^{\bullet}]/dt = 0$, then from eq 14 we have

$$[HO^{\bullet}] = \frac{k_1[Fe^{2+}][H_2O_2]}{k_2[AMX] + k_7[Fe^{2+}]} \quad (20)$$

To obtain an equation showing the relationship of all the species on the degradation rate of AMX, eq 20 can be substituted into eq 12 to obtain eq 21.

$$r_{AMX} = \frac{d[AMX]}{dt} = \frac{k_1k_2[AMX][Fe^{2+}][H_2O_2]}{k_2[AMX] + k_7[Fe^{2+}]} \quad (21)$$

For the purpose of simulation, eq 21 can be written in terms of initial concentration of H_2O_2 and Fe^{2+} by integrating eq 18 and eq 19 as shown in eq 22 and eq 23, respectively, and substitute into eq 21.

$$[H_2O_2] = [H_2O_2]_o\, e^{\gamma_1 t} \quad (22)$$

$$[Fe^{2+}] = [Fe^{2+}]_o\, e^{\gamma_2 t} \quad (23)$$

where γ_1 and γ_2, respectively, represent $k_1[Fe^{2+}]$ and $k_7[HO^{\bullet}]$. The equation implies that the residual concentrations of H_2O_2 and Fe^{2+} depend on their respective initial concentrations and their rate of consumption.

Then the rate of AMX degradation can be represented as follows:

$$r_{AMX} = \frac{d[AMX]}{dt} = \frac{k_1k_2[AMX][Fe^{2+}]_o\, e^{\gamma_2 t}[H_2O_2]_o\, e^{\gamma_1 t}}{k_2[AMX] + k_7[Fe^{2+}]_o\, e^{\gamma_2 t}} \quad (24)$$

When the separation of variables and integration are applied, the concentration of AMX in eq 24 becomes a function of reaction time decreasing from its initial value of $[AMX]_{t=o}$ to $[AMX]_{t=t}$ as shown in eq 25.

$$\frac{k_7[Fe^{2+}]_o}{k_1k_2[H_2O_2]_o} \ln\frac{[AMX]_o}{[AMX]} + \frac{([AMX]_o - [AMX])}{k_2[H_2O_2]_o} = \left(\frac{1 - e^{-(\gamma_1+\gamma_2)t}}{(\gamma_1+\gamma_2)}\right) \quad (25)$$

Equation 25 shows that in a typical photo-Fenton process, the overall degradation efficiency depends more on the four process parameters (i.e., H_2O_2 dosage, AlPMC loading, reaction time, and initial concentration of AMX) that were earlier studied with ANN and optimized using the RSM. As it was earlier noted, the contributory effects of state functions like temperature, UV irradiation, and agitation were assumed to be lumped up into k_2 as shown by eq 26.

$$k_2 = k_2' + k_2(T) + k_2(UV) + k_2(rpm) \quad (26)$$

where k_2', $k_2(T)$, $k_2(UV)$, $k_2(rpm)$ are the rate constant due to the concentration of the reactants, temperature, UV irradiation, and agitation, respectively. Determination of individual k values was not considered in this study. For simplification, the terms of eq 25 can be lumped as shown in eq 27:

$$\alpha \ln\frac{[AMX]_o}{[AMX]} + \beta([AMX]_o - [AMX]) = \left(\frac{1 - e^{-\delta t}}{\delta}\right) \quad (27)$$

where $\alpha = (k_7[Fe^{2+}]_o)/(k_1k_2[H_2O_2]_o)$, $\beta = 1/(k_2[H_2O_2]_o)$ and $\delta = (\gamma_1 + \gamma_2)$.

The above set of equations established a new kinetic model for the optimized degradation process of AMX in a photo-Fenton process.

4.4.2. Verification of the New Kinetic Model Accuracy. The accuracy of the new kinetic model was tested on the optimized two significant variables (AlPMC loading and H_2O_2 dosage) in ANN studies. Figure 6 compares the experimental and the modeled residual concentration of AMX at different AlPMC loading and time. The new kinetic model showed the highest

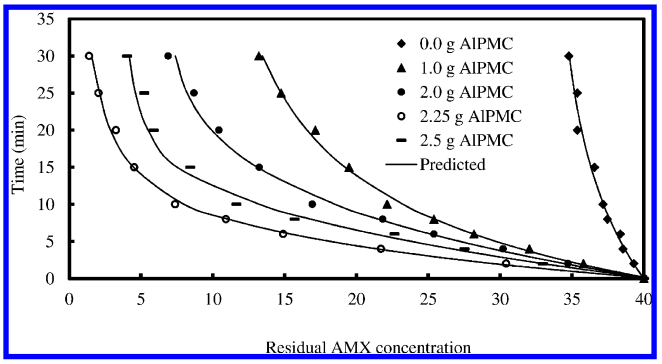

Figure 6. The effect of AlPMC loading on AMX residual concentration fitted by the developed kinetic model and the experimental observed values; $[AMX]_o$ = 40 ppm, $[H_2O_2]_o$ = 15% excess H_2O_2, temperature = 30 °C.

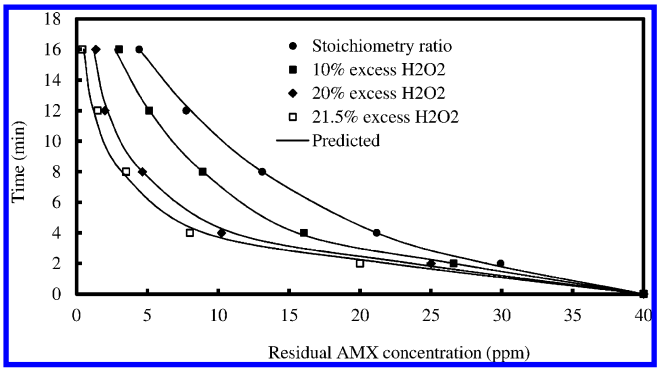

Figure 7. The effect of H_2O_2 dosage on AMX residual concentration fitted by the new kinetic model; $[AMX]_o$ = 40 ppm, temperature = 30 °C, AlPMC loading = 2.25 g.

R^2 of 0.999 in 0.0 g AlPMC loading but this cannot be used to validate the model because the quantity $k_7[Fe^{2+}]_o/k_1k_2[H_2O_2]_o$ is equal to zero in this condition, hence the high correlation may be due to mere mathematical coincidence. Both 1.0 and 2.0 g AlPMC loading showed 0.987 while 2.25 g showed 0.989, but 2.5 g showed the least R^2 value of 0.953. The results of k_2 obtained from the model are shown in Table 2. As the AlPMC dosage is increased from 1.0 to 2.25 g, the value of k_2 increased from 57.11 to 122.5 M^{-1} S^{-1}. Further increment of AlPMC to 2.5 g decreased the value of k_2 to 107.9 M^{-1} S^{-1}. The initial increment in k_2 is due to the availability of more catalyst active sites for the generation of $HO^{\bullet}$ as earlier noted, while the reduction in the value of k_2 at 2.5 g of AlPMC loading could be because it was in excess of the optimized dosage for 40 ppm AMX concentration. Therefore, it can be concluded that at this prevailing condition R7 in the chain termination stage with a very high rate constant is dominating the reaction process via ferrous ion scavenging on $HO^{\bullet}$[10,17,24] leading to a decrease in the degradation rate of AMX.

The result of effect of H_2O_2 dosage on residual AMX tested with the new kinetic model is shown in Figure 7 with average R^2 value of 0.989. It was observed that as the degradation time increases, the residual AMX concentration decreases. The value of k_2 (Table 2) increased with an increase in H_2O_2 dosage from the stoichiometric ratio up to the optimized dosage. This confirmed that the mathematical model satisfactorily and adequately described the influence of the H_2O_2 dosage over the experimental scope on which the model is based. The results obtained from this new kinetic model were in accordance with the trend observed in the ANN and optimization (RSM) studies.

5. CONCLUSION

Catalyst loading and H_2O_2 dosage have been revealed by artificial neural network modeling to be the most significant input variables affecting the degradation of AMX in the heterogeneous photo-Fenton process. The optimization study using response surface methodology also confirmed this same observation. The optimum condition to degrade 97.87% of 40 ppm of AMX was 21.54% excess H_2O_2 dosage, 2.24 g of AlPMC in 10 min degradation time. The experimental validation result showed a variation of 2.47%, probably due to some interference during laboratory studies. The mathematical model developed for the degradation kinetics showed high R^2 values signifying a strong degree of correlation. Both the result of AlPMC loading and H_2O_2 dosage showed enhanced increase in the rate of AMX degradation as shown by the rate constants for AMX degradation evaluated from the developed mathematical model.

■ ASSOCIATED CONTENT

Supporting Information

Table S1, factors to be optimized using D-Optimal design; Table S2, comparison of 10 different back-propagation algorithms with 5 neurons in the hidden layer; Table S3, evaluation of possible combinations of input variables; Table S4, Experimental design and response based on experimental runs proposed by D-Optimal design for AMX degradation with AlPMC; Table S5, ANOVA test for the response model *Y* (AMX % degradation); Figure S1, parity plot comparing the actual AMX degradation data with the model predictions; Figure S2, diagnostics AMX response model: (a) normal probability of residuals, (b) internally outliers' T points. This material is available free of charge via the Internet at http://pubs.acs.org.

■ AUTHOR INFORMATION

Corresponding Author

*Tel.: +60164955453. E-mail: ayodele_olumide@yahoo.com.

Notes

The authors declare no competing financial interest.

■ ACKNOWLEDGMENTS

O.B. Ayodele acknowledges the scholarship grant provided by the Niger Delta Development Commission (NDDC), Port Harcourt, Nigeria.

Table 2. Rate of Hydroxyl Radical Attack on AMX

	AlPMC (g)					H_2O_2 (% excess)			
dosage	0	1.0	2.0	2.25	2.5	stoic ratio	10	20	21.5
k_2 (M^{-1} S^{-1})	12.55	57.11	97.38	122.5	107.9	87.45	98.05	110.2	122.5

REFERENCES

(1) Bound, J. P.; Voulvoulis, N. Predicted and measured concentrations for selected pharmaceuticals in UK rivers: Implications for risk assessment. *Water Res.* **2006**, *40*, 2885.

(2) Rozas, O.; Contreras, D.; Mondaca, M. A.; Perez-Moyac, M.; Mansilla, H. D. Experimental design of Fenton and photo-Fenton reactions for the treatment of ampicillin solutions. *J. Hazard. Mater.* **2010**, *177*, 1025.

(3) Elmolla, E. S.; Chaudhuri, M.; Eltoukhy, M. M. The use of artificial neural network (ANN) for modeling of COD removal from antibiotic aqueous solution by the Fenton process. *J. Hazard. Mater.* **2010**, *179*, 127.

(4) Ayodele, O. B.; Lim, J. K.; Hameed, B. H. Degradation of phenol in photo-Fenton process by phosphoric acid modified kaolin supported ferric-oxalate catalyst. *Chem. Eng. J.* **2012**, *197*, 181.

(5) Trovo, A. G.; Melo, A. S. S.; Nogueira, R. F. P. Photodegradation of the pharmaceuticals amoxicillin, bezafibrate and paracetamol by the photo-Fenton process—Application to sewage treatment plant effluent. *J. Photochem. Photobiol. A: Chem.* **2008**, *198*, 215.

(6) Trovó, A. G.; Nogueira, R. F. P.; Aguera, A.; Fernandez-Alba, A. R.; Malato, S. Degradation of the antibiotic amoxicillin by photo-Fenton process—Chemical and toxicological assessment. *Water Res.* **2011**, *45*, 1394.

(7) Dopar, M.; Kusic, H.; Koprivanac, N. Treatment of simulated industrial wastewater by photo-Fenton process. Part I: The optimization of process parameters using design of experiments (DOE). *Chem. Eng. J.* doi:10.1016/j.cej.2010.09.070.

(8) Malato, S.; Fernandez-Ibanez, P.; Maldonado, M. I.; Blanco, J.; Gernjak, W. Decontamination and disinfection of water by solar photocatalysis: Recent overview and trends. *Catal. Today.* **2009**, *147*, 1.

(9) Kasiri, M. B.; Aleboyeh, H.; Aleboyeh, A. Modeling and optimization of heterogeneous photo-fenton process with response surface methodology and artificial neural networks. *Environ. Sci. Technol.* **2008**, *42*, 7970.

(10) Wu, Y.; Zhou, S.; Qin, F.; Zheng, K.; Ye, X. Modeling the oxidation kinetics of Fenton's process on the degradation of humic acid. *J. Hazard. Mater.* **2010**, *179*, 533.

(11) Montogomery, D. C. *Design and Analysis of Experiments*; John Wiley and Sons: New York, 2005.

(12) Myer, R. H.; Montogomery, D. C. *Response Surface Methodology: Process and Product Optimization using Designed Experiment*, 2nd ed.; John Wiley and Sons: New York, 2002.

(13) Moral, H.; Aksoy, A.; Gokcay, C. F. Modeling of the activated sludge process by using artificial neural networks with automated architecture screening. *Comput. Chem. Eng.* **2008**, *32*, 2471.

(14) Daneshvar, N.; Khataee, A. R.; Djafarzadeh, N. The use of artificial neural networks (ANN) for modeling of decolorization of textile dye solution containing C. I. Basic Yellow 28 by electrocoagulation process. *J. Hazard. Mater.* **2006**, *B137*, 1788.

(15) Aleboyeh, A.; Kasiri, M. B.; Olya, M. E.; Aleboyeh, H. Prediction of azo dye decolorization by UV/H_2O_2 using artificial neural networks. *Dyes Pigm.* **2008**, *77*, 288.

(16) Oguza, E.; Tortum, A.; Keskinler, B. Determination of the apparent rate constants of the degradation of humic substances by ozonation and modeling of the removal of humic substances from the aqueous solutions with neural network. *J. Hazard. Mater.* **2008**, *157*, 455.

(17) Ayodele, O. B.; Lim, J. K.; Hameed, B. H. Pillared montmorillonite supported ferric oxalate as heterogeneous photo-Fenton catalyst for degradation of amoxicillin. *Appl. Catal., A* **2012**, *413– 414*, 301.

(18) Katsumata, H.; Okada, T.; Kaneco, S.; Suzuki, T.; Ohta, K. Degradation of fenitrothion by ultrasound/ferrioxalate/UV system. *Ultrason. Sonochem.* **2010**, *17*, 200.

(19) Bautitz, I. R.; Pupo Nogueira, R. F. Photodegradation of lincomycin and diazepam in sewage treatment plant effluent by photo-Fenton process. *Catal. Today.* **2010**, *151*, 94.

(20) Slokar, Y. M.; Zupanb, J.; Marechal, A. M. L. The use of artificial neural network (ANN) for modeling of the H_2O_2/UV decoloration process: part I. *Dyes Pigm.* **1999**, *42*, 123.

(21) Multifactor RSM Tutorial (Part 2—Optimization). *Design-Expert 8 User's Guide*, version 7.1.5; Stat Ease: Minneapolis, MN, 2008.

(22) Yetilmezsoy, K.; Demirel, S.; Vanderbei, R. J. Response surface modeling of Pb(II) removal from aqueous solution by Pistacia vera L.: Box—Behnken experimental design. *J. Hazard. Mater.* **2009**, *171*, 551.

(23) Diya'uddeen, B. H.; Abdul-Aziz, A. R.; Daud, W. M. A. Oxidative mineralization of petroleum refinery effluent using Fenton-like process., *Chem. Eng. Res. Des.* 10.1016/j.cherd.2011.06.010.

(24) Daud, N. K.; Hameed, B. H. Fenton-like oxidation of reactive Black 5 solution using iron Montmorillonite K10 catalyst. *J. Hazard. Mater.* **2010**, *176*, 1118.

(25) Wu, F.; Li, J.; Peng, Z. E.; Deng, N. Photochemical formation of hydroxyl radicals catalyzed by montmorillonite. *Chemosphere.* **2008**, *72*, 407.

(26) De León, M. A.; Castiglionia, J.; Bussi, J.; Sergio, M. Catalytic activity of an iron-pillared montmorillonitic clay mineral in heterogeneous photo-Fenton process. *Catal. Today.* **2008**, *133—135*, 600.

(27) Daud, N. K.; Hameed, B. H. Decolorization of Acid Red 1 dye solution by Fenton-like process using Fe—Montmorillonite K10 catalyst. *Chem. Eng. J.* **2010**, *165*, 111.

(28) Liu, X. D.; Lu, X. C. A thermodynamic understanding of clay-swelling inhibition by potassium ions. *Angew. Chem., Int. Ed.* **2006**, *45* (38), 6300.

(29) Neyens, E.; Baeyens, J. A review of classic Fenton's peroxidation as an advanced oxidation technique. *J. Hazard. Mater.* **2003**, *98*, 33—50.